Imposing Navier-slip boundary conditions on the lattice Boltzmann equation in three dimensions

Zainab Ali Bu sinnah[a], David I. Graham[b] and Tim Reis [c]

[a]Department of Mathematics, University Colleges at Nairiyah, University of Hafr Albatin (UHB), Hafr Al-Batin 31991, Saudi Arabia;
[b]School of Engineering, Computing and Mathematics, Plymouth University, PL4 8AA, UK,
[c]School of Computing and Mathematical Sciences, University of Greenwich, SE10 9LS,UK
.

ARTICLE HISTORY
Compiled July 23, 2025

ABSTRACT
Moment-based boundary conditions for the lattice Boltzmann equation are extended to Navier-slip flow in three dimensions. The slip velocity is proportional to the velocity gradient at the wall and imposed locally within the moment system. To capture gradients at edges the first order contributions to the third velocity moments are retained. The proposed methodology is validated by computing solutions to pulsatile and duct flows and second order accuracy is confirmed.

KEYWORDS
Lattice Boltzmann method; moment-based boundary conditions; Navier-slip.

1. Introduction

The lattice Boltzmann method (LBM) is usually considered to be a mesoscopic numerical method that can be used to compute solutions to the Navier-Stokes equations. Boundary conditions have been implemented in the lattice Boltzmann algorithm in many ways. The bounce-back scheme and its direct variants are the most common, where at a no-slip wall the (discrete) velocity distribution functions reverse their velocity and return to the computational node they came from. While being unquestionably useful, the method generates a viscosity dependent error when used with the popular single relaxation time model [13, 18]. To remove this artefact a multiple relaxation time collision operator with judiciously chosen parameters is needed [11, 14, 15]. To extend the method to slip conditions, a combination of bounce back and specular reflection boundary conditions, or diffusive boundary conditions, have been proposed [8, 22, 41, 42, 44], but the numerical slip error with a single relaxation time model remains.

For example, kinetic boundary conditions [3] can derived directly from kinetic theory to extend the LBM to flows with slip at walls. Some of these methods incorporate a

CONTACT: Zainab Bu sinnah Email: zabusinnah@uhb.edu.sa

tangential slip velocity by adjusting the distribution functions as follows:

$$f_i = f_i^{\text{eq}} + \Delta f_i(u_{\text{slip}}) \tag{1}$$

This formats the equilibrium distribution f_i^{eq} and the correction term Δf_i as a function of slip velocity u_{slip}. Other lattice Boltzmann boundary conditions employ a parameter r to determine the slip velocity and reduce viscosity-dependent errors. This is achieved through combinations such as bounce-back with specular reflection or diffusive boundary conditions [42], [41], [22].

$$f_i = r f_i^{BB} + (1 - r)\, f_i^{SR \text{ or } D},\ 0 < r < 1 \tag{2}$$

In the specular reflection (SR) boundary condition, unknown distribution functions reflect in the same manner as light reflecting off a mirror. In the diffusive (D) boundary condition, unknown distributions are replaced by a Maxwell-Boltzmann equilibrium distribution, with wall velocity imposed and density chosen such that there is no net mass flux at the wall. All of these methods, despite showing promise in application, are prone to numerical artefacts on the vicinity of boundaries including numerical slip.

Chai et al. [8] pioneered the approach of combining bounce-back and full diffusive boundary conditions for the LBM to study microscale gas flows. With this method they explored how surface roughness effects gas flow within microchannels. They found that surface roughness has a significant impact on mass flow rate and friction factor, particularly at low Knudsen numbers where gas-surface interactions are more pronounced. As the Knudsen number increases and the flow becomes more rarefied, the effect of surface roughness decreases. Chai *et al.* [9] extended their approach to multiple-relaxation-time collision operators that could be tailored for gas flow over arrays of cylinders. They studied unwanted discrete effects on slip conditions, which are particularly prevalent as the local Knudsen number increases.

Significant progress in the study of lattice Boltzmann methods for slip flow has been made by Silva and coworkers in recent years [36–38]. Their detailed analysis highlights numerical artefacts that are present in LBMs and how one can use two-relaxation-time approaches to control them. They extend the local second-order boundary (LSOB) method to incorporate slip in geometrically complicated boundaries in 2 and 3 dimensions. Thus the method of Silva *et. al* may be considered state-of-the-art theoretical work that has the potential to be useful in many applications.

Tae *et. al.* [43] presented an interface-resolved lattice Boltzmann examination of how a unilateral slippery (single-slip) bottom wall influences the inertial migration of neutrally buoyant particles in channel flow. In contrast to symmetric channels, where particles typically bifurcate around the centreline, the presence of the slip wall shifts the critical equilibrium position below the centreline. They found that particles tend to migrate toward the mid-height of the channel at higher Reynolds numbers, whereas an increase in slip length causes the lower equilibrium position to draw particles closer to the slip wall.

Samanta *et. al.* [33] studied lid-driven cavity flow with slip boundary conditions using the lattice Boltzmann method. They considered flows with a tangential momentum accommodation coefficient that varied from 0.01 to 1 and Reynolds numbers from 20 to 300. Two boundary condition implementations - the tangential momentum accommodation coefficient (TMAC) method and the modified bounce-back specular reflection (MBSR) method - were compared, with MBSR predicting higher slip velocities. Their results show that increasing slip suppresses secondary vortex formation.

Additionally, greater slip causes the primary vortex to shift toward the cavity centre. We note in passing that Mohammed and Reis [26] used the moment-based methodology to study rarefied lid driven cavity flow with slip conditions and showed good agreement between LBM and benchmark data, including DSMC results.

The moment-based approach [5] is an extension of the ideas of Noble *et al.* [28] and aims to impose hydrodynamic boundary conditions precisely at lattice grid points by translating constraints on the moments into constraints on the distribution functions. To do this consistently, one requires the same number of linearly independent moment constraints as unknown distribution functions at a boundary. This methodology allows no-slip conditions to be imposed precisely at grid points and slip conditions locally with a high level of accuracy (free from numerical, or artificial, slip) [7, 25, 26, 30–32, 39].

Guo and Hou [16] evaluated bounce-back, non-equilibrium bounce back (NEBB), and moment-based schemes for the discrete unified gas kinetic scheme (DUGKS). Their simulations of Couette flow, Poiseuille flow, and Rayleigh–Taylor instabilities demonstrated second-order accuracy of these methods, and the showed that the moment-based scheme consistently outperformed bounce back and NEBB conditions in terms of accuracy, efficiency, including their extension to multiphase flow applications. Bazarin *et al.* [4] address the challenges of boundary conditions in the lattice Boltzmann method with a focus on moments-based models. They explored various manifestations of a generalised moment-based approach, including some that lead to an over-determined system, and argued for an optimal approach in terms of accuracy, mass conservation, convergence, and stability based on the two-dimensional lid-driven cavity flow.

The current shortcoming of the moment-based approach to lattice Boltzmann boundary conditions is geometric flexibility, but a step forward was made by Krastins *et al.* [21] who extended the methodology to no-slip flows in three dimensions. Added difficulties for the moment-based approach in three dimensions are edges, where two faces (boundary planes) meet, and corners, where three faces meet. Krastins *et al.* required the third moment - a non hydrodynamic moment - to impose no slip conditions and faces edges and corners in 3D and neglected their non-equilibrium contributions.

In this paper we build on Krastins *et al.* [21] and Mohammed *et al.* [25] and present a moment-based approach for imposing Navier-slip conditions on the lattice Boltzmann equation in three dimensions. We are concerned only with Navier-slip here, where the slip length is not related to a Knudsen number. We simulate flows with known analytical solutions to assess the accuracy of the proposed scheme. The remainder of this paper is structured as follows. In Section 2 we briefly discuss the D3Q19 LBM and remind the reader of the relationship between the LBM and the Navier-Stokes equations, including an overview of the methodology of moment-based boundary conditions for Navier-slip conditions in three dimensional LBMs. In Section 3 we present the method and results for three dimensional pulsatile flow and in Section 4 we study flow inside a square duct with our new method. Concluding remarks left for Section 5.

2. The discrete Boltzmann equation

The discrete velocity Boltzmann equation with a single relaxation time is

$$\partial_t f_i + \boldsymbol{c}_i . \bigtriangledown f_i = -\frac{1}{\tau}(f_i - f_i^0) + F_i \tag{3}$$

where $f_i(\boldsymbol{x}, t)$ is the particle velocity distribution function with discrete particle velocity $\boldsymbol{c}_i$. The finite set $\boldsymbol{c}_i : i = 0, \ldots, b$ form an integer lattice, such as the $D3Q19$ lattice shown in Figure 1. The F_i accounts for additional body forces. The left hand side of equation (3) describes advection of f_i by the velocity $\boldsymbol{c}_i$ and the right hand side (the collision term) says that the f_i relax to their equilibria f_i^0 over the timescale τ. The equilibria are algebraic and given by [17],

$$f_i^0 = \omega_i \rho \left(1 + \frac{\boldsymbol{c}_i.\boldsymbol{u}}{c_s^2} + \frac{(\boldsymbol{c}_i.\boldsymbol{u})^2}{2c_s^4} - \frac{\boldsymbol{u}^2}{2c_s^2} \right), \tag{4}$$

where ρ is the fluid density, $\boldsymbol{u}$ is the velocity of the fluid, and c_s is the speed of sound, which for the D3Q19 lattice considered here is $1/\sqrt{3}$. The weights, ω_i, for the D3Q19 lattice are

$$\omega_i = \begin{cases} \frac{1}{3} & i = 0 \\ \frac{1}{18} & i = 1, \ldots, 6 \\ \frac{1}{36} & i = 7, \ldots, 18 \end{cases}$$

The force term, F_i, is given by [23]

$$F_i = \omega_i \rho \left(\frac{\boldsymbol{c}_i.\boldsymbol{g}}{c_s^2} + \frac{(\boldsymbol{c}_i.\boldsymbol{u})\,(\boldsymbol{c}_i.\boldsymbol{g})}{c_s^4} - \frac{(\boldsymbol{g}.\boldsymbol{u})}{c_s^2} \right). \tag{5}$$

where $\boldsymbol{g}$ is the body force being imposed.

Mass and momentum are defined to be the first two discrete particle velocity moments of f_i and are conserved by collisions:

$$\rho = \sum_i f_i = \sum_i f_i^0, \quad \rho \boldsymbol{u} = \sum_i f_i \boldsymbol{c_i} = \sum_i f_i^0 \boldsymbol{c}_i.$$

The momentum flux tensor is not conserved and is defined to be $\boldsymbol{\Pi} = \sum_i f_i \boldsymbol{c}_i \boldsymbol{c}_i$. For later use we also define the third moment, which is a non-conserved non-hydrodynamic moment, $\boldsymbol{Q} = \sum_i f_i \boldsymbol{c}_i \boldsymbol{c}_i \boldsymbol{c}_i$.

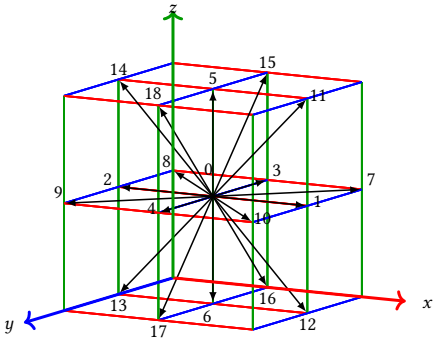

Figure 1. D_3Q_{19} Lattice

2.1. *Recovering the Navier-Stokes equation from the discrete velocity Boltzmann equation*

Taking the zero, first and second order discrete velocity moments of the discrete velocity Boltzmann equation (3) yields

$$\partial_t \rho + \nabla . \rho \boldsymbol{u} = 0, \tag{6}$$
$$\partial_t (\rho \boldsymbol{u}) + \nabla . \boldsymbol{\Pi} = \boldsymbol{g}, \tag{7}$$
$$\partial_t \boldsymbol{\Pi} + \nabla . \boldsymbol{Q} = -\frac{1}{\tau}(\boldsymbol{\Pi} - \boldsymbol{\Pi}^0) + \boldsymbol{ug} + \boldsymbol{gu}, \tag{8}$$

If one now applies the following Chapman-Enskog scales expansion to the non-conserved moments and the time derivatives,

$$\boldsymbol{\Pi} = \boldsymbol{\Pi}^0 + \tau \boldsymbol{\Pi}^1 + O(\tau^2), \quad \boldsymbol{Q} = \boldsymbol{Q}^0 + \tau \boldsymbol{Q}^1 + O(\tau^2), \quad \partial_t = \partial_{t_0} + \tau \partial_{t_1} + O(\tau^2). \tag{9}$$

then, after some algebra and neglecting terms of $O(\tau^2)$ and $O(u^3)$, one arrives at the (weakly compressible) Navier-Stokes equations [31]

$$\partial_t \rho + \nabla . \rho \boldsymbol{u} = 0, \tag{10}$$
$$\partial_t (\rho \boldsymbol{u}) + \nabla . \left(pI + \rho \boldsymbol{uu} \right) = \nabla . \mu \left[(\nabla \boldsymbol{u}) + (\nabla \boldsymbol{u})^T \right] + \boldsymbol{g}, \tag{11}$$

where $p = \rho c_s^2$ is the pressure and $\mu = \tau \rho c_s^2$ is dynamic viscosity. In obtaining the above we used the equilibrium moments

$$\boldsymbol{\Pi}^0_{\alpha\beta} = p\delta_{\alpha\beta} + \rho u_\alpha u_\beta, \tag{12}$$
$$Q^0_{\alpha\beta\gamma} = \rho c_s^2 \left(u_\gamma \delta_{\alpha\beta} + u_\beta \delta_{\alpha\gamma} + u_\alpha \delta_{\gamma\beta} \right), \tag{13}$$

and obtained the first order (in τ) correction to $\boldsymbol{\Pi}$,

$$\boldsymbol{\Pi}^1_{\alpha\beta} = -\rho c_s^2 \left(\partial_\alpha u_\beta + \partial_\beta u_\alpha \right) + O(u^3). \tag{14}$$

It is worth reminding the reader that we have recovered the weakly compressible Navier-Stokes equations but with errors of order u^3 and τ^2. The cubic errors are small by the small Mach number assumption, and clearly we require $u \ll c_s$, where c_s is the sound speed. Similarly, large values of the relaxation time τ would mean that neglecting higher order terms in the expansion would lack justification and the model would not be expected to be a very accurate Navier-Stokes solver.

While not needed directly to obtain the Navier-Stokes equations, we also find the first order correction to $\boldsymbol{Q}$ to be

$$Q^1_{\alpha\beta\gamma} = \rho c_s^2 \left[u_\gamma \delta_{\alpha\beta} + u_\beta \delta_{\alpha\gamma} + u_\alpha \delta_{\beta\gamma} \right] \partial_\delta u_\delta + \rho c_s^2 \left[\delta_{\alpha\beta} \partial_\gamma + \delta_{\alpha\gamma} \partial_\beta + \partial_\alpha \delta_{\gamma\beta} \right] u_\theta u_\theta$$
$$+ \frac{\rho c_s^2}{2} \left[u_\alpha \left(\partial_\beta u_\gamma + \partial_\gamma u_\beta \right) + u_\gamma \left(\partial_\alpha u_\beta + \partial_\beta u_\alpha \right) + u_\beta \left(\partial_\alpha u_\gamma + \partial_\gamma u_\alpha \right) \right]. \tag{15}$$

2.2. The lattice Boltzmann equation

Now convinced that the Navier-Stokes equations are embedded within the moments of the discrete velocity Boltzmann equation, we discretise equation (3) in space and time by integrating it over a characteristic for time Δt, and using the Trapezoidal Rule to approximate the resulting integral on the right hand side. This yields

$$\overline{f}_i\left(\boldsymbol{x}+\boldsymbol{c}_i\Delta t, t+\Delta t\right)-\overline{f}_i\left(\boldsymbol{x},t\right)=-\frac{1}{\overline{\tau}}\left[\left(\overline{f}_i\left(\boldsymbol{x},t\right)-f_i^0\left(\boldsymbol{x},t\right)\right)-\tau F_i\right], \tag{16}$$

where $\overline{\tau}=\dfrac{\tau+0.5\Delta t}{\Delta t}$ and we have used the He *et al.* [17] variable transform

$$\overline{f}_i=f_i+\frac{\Delta t}{2\tau}\left(f_i-f_i^0\right)-\frac{\Delta t}{2}F_i. \tag{17}$$

Macroscopic variables can be easily obtained from moments of the transferred variable, $\overline{f}_i$:

$$\begin{aligned}
\overline{\rho}&=\sum_i\overline{f}_i=\rho\\
\overline{\rho\boldsymbol{u}}&=\sum_i\boldsymbol{c}_i\overline{f}_i=\rho\boldsymbol{u}+\rho\frac{\Delta t}{2}\boldsymbol{F}\\
\overline{\boldsymbol{\Pi}}&=\sum_i\boldsymbol{c}_i\boldsymbol{c}_i\overline{f}_i=\frac{2\tau+\Delta t}{2\tau}\boldsymbol{\Pi}-\frac{\Delta t}{2\tau}\boldsymbol{\Pi}^0-\frac{\Delta t}{2}\left(\boldsymbol{g}\boldsymbol{u}+\boldsymbol{u}\boldsymbol{g}\right)\\
\overline{\boldsymbol{Q}}&=\sum_i\boldsymbol{c}_i\boldsymbol{c}_i\boldsymbol{c}_i\overline{f}_i=\frac{2\tau+\Delta t}{2\tau}\boldsymbol{Q}-\frac{\Delta t}{2\tau}\boldsymbol{Q}^0-\sum_i\boldsymbol{c}_i\boldsymbol{c}_i\boldsymbol{c}_iF_i.
\end{aligned} \tag{18}$$

2.3. Moment-based methodology for boundary conditions in three dimensions

We first discuss the extension of moment-based boundary condition to three dimensions with non-slip boundary conditions, as considered by Krastins *et al.*[21], before highlighting the necessary adjustments and extensions to incorporate slip.

At a flat boundary aligned with gridpoints the velocity distribution functions f_i that have (particle) velocities tangential to the boundary, or in the direction pointing out of the domain, are known, while those with velocity pointing into the domain are unknown and need to be supplied. The moment-based approach provides a way of finding the unknown f_i through constraints on moments. It identifies groups of moments with the same linear combination of incoming (unknown) f_i and imposes a boundary condition on one moment from each linearly independent group [5]. The resulting linear system to be solved is very small and only needs to be computed once, before the simulation.

In two dimensions, one can impose physically meaningful boundary conditions on hydrodynamic moments only (that is, on moments which have a direct physical interpretation in terms of the Naiver-Stokes description of flow) [2, 24, 32]. Krastins *et al.* [21] attempted the same methodology in 3D with the $D3Q19$ lattice. Here there are five, nine and twelve unknown incoming distributions at the planar boundary faces,

edges and corners, respectively, and the same number of independent moment conditions for the respective boundaries are required. The moment groups are shown in full for a boundary face at the south of a computational domain, an edge at the south west, and a front facing south west corner in Tables 1, 2, and 3, respectively, in the appendix. Note that this is the case only when the boundaries are aligned vertically or horizontally with lattice grid points. More complicated boundaries is a topic for further research.

Krastins *et al.* [21] argued that at edges and corners there are more unknown f_i than hydrodynamic moments. They used the third moment, $\boldsymbol{Q}$, to close the system, considering lattice symmetries when doing so, and assumed that non-equilibrium contributions to $\boldsymbol{Q}$ in equation (15) can be neglected. Recall that only zero velocity boundary conditions were under consideration in Krastins *et al.* For the flows under consideration in this article, the tangential velocity does not vanish at a boundary. For this reason, we use in our boundary conditions the first non-equilibrium contribution to $\boldsymbol{Q}$, which include spatial derivatives in its expression.

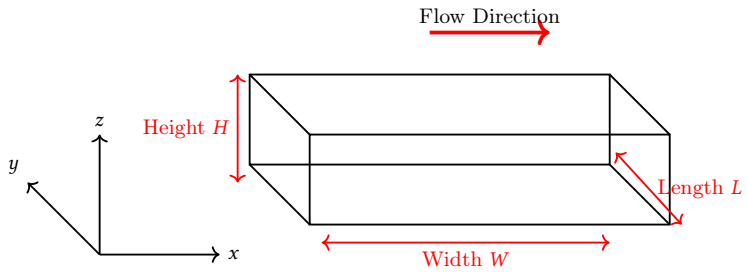

Figure 2. Illustration of the flow domain.

2.4. Navier slip boundary condition.

In 1823, Navier proposed a slip boundary condition which assumed that tangential fluid velocity a surface, u_s, to be proportional to the rate of shear stress at the surface [27]. That is,

$$u_s = L_s \frac{\partial u}{\partial n}\bigg|_{\text{surface}}, \tag{19}$$

where u is tangential fluid velocity, L_s is the slip length, n is the outward normal direction to the surface. This boundary condition has found applications in flow over rough surfaces [19], polymer processing [12], and lubricating flows [6], for example, and it is this condition that we will impose on three dimensional lattice Boltzmann methods using the moment-based approach.

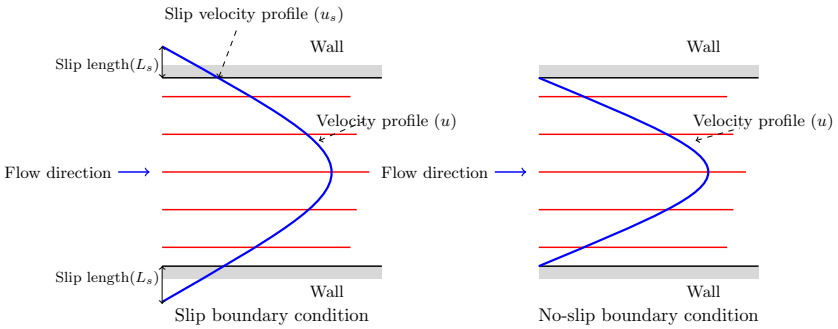

Figure 3. No slip velocity and slip velocity with slip length.

3. Three dimensional pulsatile flow with Navier slip conditions

We simulate three dimensional pulsatile flow with Navier slip to validate our method. The flow is driven by a constant body force and is periodic in the flow direction, as shown in Figure 2. The moment-based approach is used to apply Navier-slip boundary conditions on the four solid boundaries as shown in Figure 2.

At the south face the unknown (incoming) distribution functions are $\overline{f}_5$, $\overline{f}_{11}$, $\overline{f}_{14}$, $\overline{f}_{15}$, and $\overline{f}_{18}$. The five independent moments (containing independent combinations of these unknowns) are chosen from Table 1:

$$\begin{aligned}
\rho u_x &= \rho u_s, \\
\rho u_y &= 0, \\
\rho u_z &= 0, \\
\Pi_{xx} &= \Pi^0_{xx} = \rho c_s^2 + \rho u_s^2 \\
\Pi_{yy} &= \Pi^0_{yy} = \rho c_s^2
\end{aligned} \tag{20}$$

In the above, the components of the momentum flux tensor are set to equilibrium because ($\partial_x u_x = \partial_y u_y = 0$ at the faces (see equation (14)). The body force is formed as $\mathbf{g} = (\rho g_x, 0, 0)$.

The conditions above are for the hydrodynamic moments of f_i, but recall that we are using a lattice Boltzmann algorithm for the transformed variable, $\overline{f_i}$, as defined in equation (17). Thus, the conditions on physical moments are translated to the "barred" moments (see 18) as

$$\begin{aligned}
\rho \overline{u}_x &= \rho u_s - \frac{\Delta t}{2} \rho g_x, \\
\rho \overline{u}_y &= 0, \\
\rho \overline{u}_z &= 0, \\
\overline{\Pi}_{xx} &= \rho c_s^2 + \rho u_s^2 - \Delta t \rho g_x, \\
\overline{\Pi}_{yy} &= \rho c_s^2,
\end{aligned} \tag{21}$$

As an explicit example, one can solve the linear system for the incoming distribution functions at the south face and find

$$\begin{aligned}
\overline{f}_5 &= \overline{f}_1 + \overline{f}_2 + \overline{f}_3 + \overline{f}_4 + \overline{f}_6 + 2\overline{f}_7 + 2\overline{f}_8 + 2\overline{f}_9 + 2\overline{f}_{10} + 2\overline{f}_{12} + 2\overline{f}_{13} + \\
&\quad 2\overline{f}_{16} + 2\overline{f}_{17} - \frac{2}{3}\rho + \Delta t \rho g_x u_s - \rho u_s^2, \\
\overline{f}_{11} &= -\overline{f}_1 - \overline{f}_7 - \overline{f}_{10} - \overline{f}_{12} + \frac{\rho}{6} - \frac{\Delta t}{4}\rho g_x - \frac{\Delta t}{2}\rho g_x u_s + \frac{1}{2}\rho u_s^2 + \frac{1}{2}\rho u_s, \\
\overline{f}_{14} &= -\overline{f}_2 - \overline{f}_8 - \overline{f}_9 - \overline{f}_{13} + \frac{\rho}{6} + \frac{\Delta t}{4}\rho g_x - \frac{\Delta t}{2}\rho g_x u_s + \frac{1}{2}\rho u_s^2 - \frac{1}{2}\rho u_s, \\
\overline{f}_{15} &= -\overline{f}_3 - \overline{f}_7 - \overline{f}_8 - \overline{f}_{16} + \frac{\rho}{6}, \\
\overline{f}_{18} &= -\overline{f}_4 - \overline{f}_9 - \overline{f}_{10} - \overline{f}_{17} + \frac{\rho}{6},
\end{aligned} \tag{22}$$

The density and tangential slip velocity at the face still need to be found, and in the moment-based approach they can be found in terms of imposed constraints and known $\overline{f}_i$. The density can be expressed in the form $\rho = \rho u_y + (\text{known } \overline{f}_i)$, because ρ and ρu_y are dependent moments (they have the same combination of unknowns - see Table 1):

$$\rho = \overline{f}_0 + \overline{f}_1 + \overline{f}_2 + \overline{f}_3 + \overline{f}_4 + 2\overline{f}_6 + \overline{f}_7 + \overline{f}_8 + \overline{f}_9 + \overline{f}_{10} + 2\overline{f}_{12} + 2\overline{f}_{13} + 2\overline{f}_{16} + 2\overline{f}_{17}, \tag{23}$$

The slip velocity u_s requires the velocity gradient, which is embedded in the non equilibrium part of Π_{xz} (see equation 14). Since u_x and Π_{xy} are in the same moment grouping in Table 1, we can follow [31] to find a local expression for the slip velocity:

$$u_s = \left(\frac{-6L_s}{\rho(2\tau+1)} \left(\overline{f}_{11} - \overline{f}_{12} + \overline{f}_{13} - \overline{f}_{14} \right) \right), \tag{24}$$

where we have used

$$\begin{aligned}
u_s &= -\frac{L_s}{\mu}\Pi_{xz}, \\
\overline{\Pi}_{xz} &= \frac{2\tau+1}{2\tau}\Pi_{xz}.
\end{aligned} \tag{25}$$

Similar expressions are found for other wall orientations. Where there is no slip, the conditions simplify with $u_s = 0$.

3.1. The exact solution to pulsatile flow

A pulsating pressure gradient can be applied via a body force $g_x = \left(2U_c\nu/h^2\right)\cos(wt)$, where U_c is the zero frequency centreline velocity case (*i.e.* Poiseuille flow), h is the the channel half-width, $w = \frac{2\pi}{P}$ is the frequency, P is the period, and ν the kinematic viscosity. The kinematic viscosity can be written in terms of the Reynolds number as $\nu = \frac{U_c h}{Re}$ where Reynolds number is defined as $Re = \frac{U_c h}{\nu}$. The solution to pulsatile flow with no slip boundary conditions in well know [45]. With Navier-slip conditions we find the analytical solution as seen in equations (26,27) and find similar topics and in these references [34],[20],[29]

The exact solution to this flow with Navier-slip conditions at $z = \pm h$ is

$$\frac{u_x(z)}{U_c} = \Re\left[\left(\frac{u_s}{U_c}\frac{\cosh\left((1+|)\,W_0\frac{z}{h}\right)}{\cosh\left((1+|)\,W_0\right)} + \frac{|}{W_0}\left(1 - \frac{\cosh\left((1+|)\,W_0\frac{z}{h}\right)}{\cosh\left((1+|)\,W_0\right)}\right)\right) e^{\frac{j2\pi t}{P}}\right], \quad (26)$$

$$\frac{u_s}{U_c} = \frac{(|-1)\,L_n \sinh\left((1+|)\,W_0\right)}{W_0\left[\cosh\left((1+|)\,W_0\right) - L_n W_0\,(1+|)\sinh\left((1+|)\,W_0\right)\right]}, \quad (27)$$

where $| = \sqrt{-1}$ and the dimensionless Womersley number is $W_0 = \sqrt{\frac{w}{2\nu}}h$. The dimensionless slip length is $L_n = \frac{L_s}{h}$. Note that the exact solutions does not dependent on the Reynolds number. In the simulations below, the values of L_n are chosen because they are similar to the slip lengths in related papers [31, 44], albeit via the Knudsen number.

3.2. Numerical results

We simulated the flow on computational grids with $n_x = n_y = 2$ and $n_z = 16, 32, 64, 128, 256, 512$. The relaxation times are given in lattice units where $\Delta_x = \Delta_t = 1$. In these units the characteristic velocity is $U_c = 0.1$.

The flow velocity computed by the LBM with moment-based slip boundary conditions and the exact solution are in a excellent agreement, as shown in Figure 4 at different slip lengths L_n and Womersley numbers W_0.

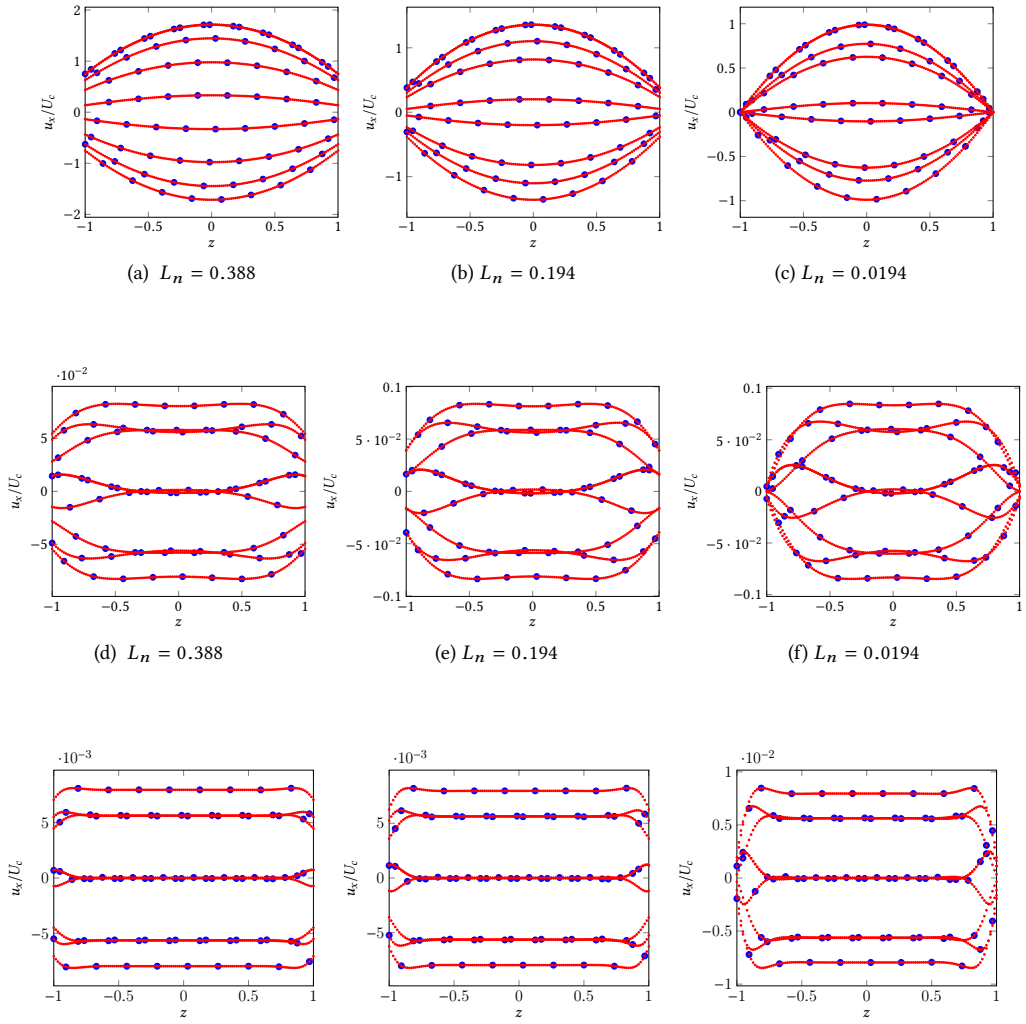

(a) $L_n = 0.388$ (b) $L_n = 0.194$ (c) $L_n = 0.0194$

(d) $L_n = 0.388$ (e) $L_n = 0.194$ (f) $L_n = 0.0194$

(g) $L_n = 0.388$ (h) $L_n = 0.194$ (i) $L_n = 0.0194, 0$

(a)

Figure 4. Blue: velocity profile of LBM; Red: velocity profile of exact solution at $\tau = 0.6$ and $n_x = n_y = 2$, $n_z = 128$. (a), (b) and (c) for $W_0 = 0.3545$; (d), (e) and (f) for $W_0 = 3.545$; (g), (h) and (i) for $W_0 = 11.201$.

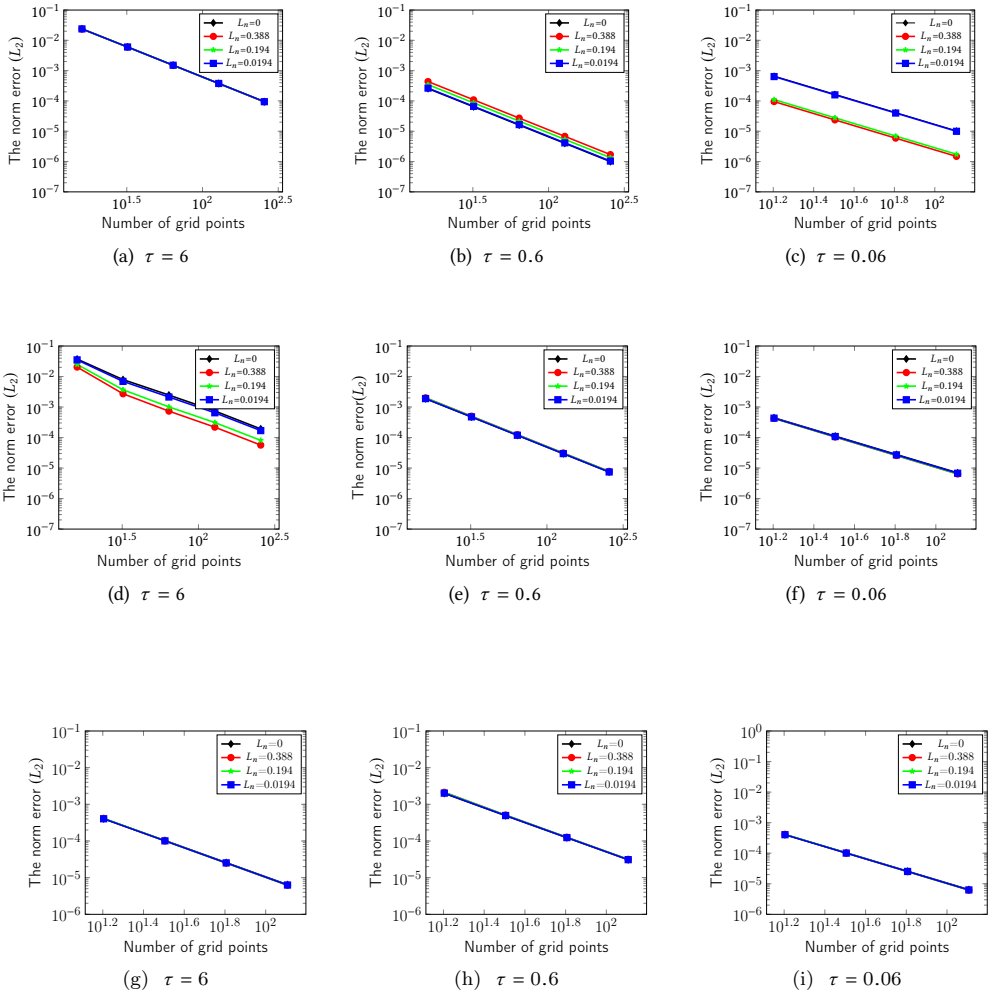

(a) $\tau = 6$ (b) $\tau = 0.6$ (c) $\tau = 0.06$

(d) $\tau = 6$ (e) $\tau = 0.6$ (f) $\tau = 0.06$

(g) $\tau = 6$ (h) $\tau = 0.6$ (i) $\tau = 0.06$

Figure 5. The global norm error for the velocity. (a), (b), (c) for $W_0 = 0.3545$, (d), (e), (f) for $W_0 = 3.545$ and (g), (h) , (i) for $W_0 = 11.201$.

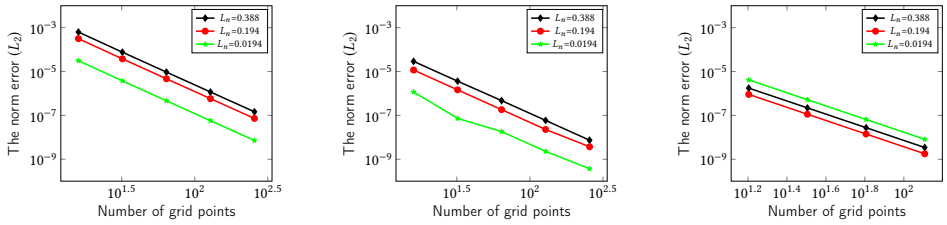

(a) $\tau = 6$ (b) $\tau = 0.6$ (c) $\tau = 0.06$

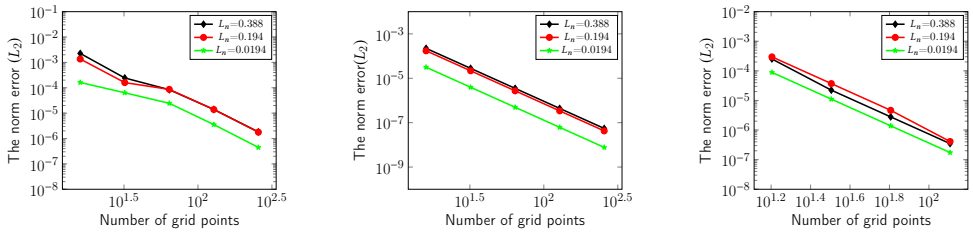

(d) $\tau = 6$ (e) $\tau = 0.6$ (f) $\tau = 0.06$

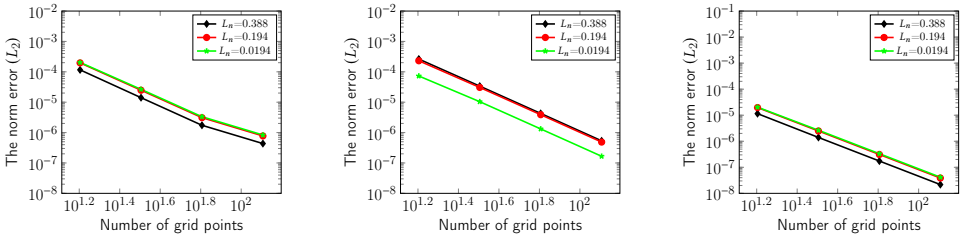

(g) $\tau = 6$ (h) $\tau = 0.6$ (i) $\tau = 0.06$

Figure 6. The norm error for slip velocity at the wall. (a), (b), (c) for $W_0 = 0.3545$ and (d), (e), (f) for $W_0 = 3.545$ and (g), (h),(i) for $W_0 = 11.201$.

The norm errors for the velocity are second order, and we note that the value of τ does not strongly effect the order of convergence, as shown in Figure 5 (b), (c), (e) and (f). Figure 6 shows the norm error of the for slip velocity at the wall. In all cases the diffusive scaling, where $\Delta_x \propto \Delta_t^2$ and the relaxation time is fixed. That is, under mesh refinement, the Reynolds number and Womersley, but not the Mach number, are fixed.

4. Laminar flow inside a rectangular duct with Navier-slip conditions

Moment-based boundary conditions are used on four confining walls to impose the Navier-slip boundary condition in the flow direction. The wall velocity is assumed to be zero in the other directions as shown in Figure 7, that is

$$u_x = u_z = 0, \quad u_y = u_s \tag{28}$$

on wall boundaries, where u_s is given by the Navier slip condition (19). A constant body force is applied in the flow direction such that $\boldsymbol{g} = (0, \rho g_y, 0)$.

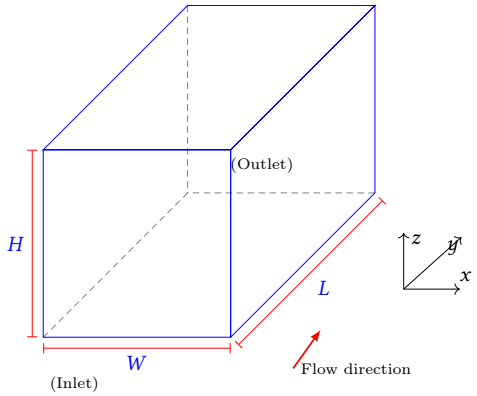

Figure 7. Illustration of the duct geometry.

4.1. Moment boundary conditions

We impose the five conditions

$$\rho u_x = \rho u_z = 0, \quad \rho u_y = \rho u_s, \quad \Pi_{xx} = \frac{\rho}{3}, \quad \Pi_{yy} = \frac{\rho}{3} + \rho u_s^2. \tag{29}$$

on the moments at face boundaries. After using the variable transformation (17) these become

$$\begin{aligned} &\rho \overline{u}_x = 0, \quad \rho \overline{u}_y = \rho u_s - \frac{\Delta t}{2} \rho g_y, \quad \rho \overline{u}_z = 0, \\ &\overline{\Pi}_{xx} = \frac{\rho}{3}, \quad \overline{\Pi}_{yy} = \frac{\rho}{3} + \rho u_s^2 - \Delta t \rho g_y, \end{aligned} \tag{30}$$

which, as in the previous section, can be solved simply for the incoming $\overline{f}_i$. Again, the density ρ and precise form of the slip velocity, u_s, can be found from known distribution functions and imposed conditions (see Section 3).

To find the unknown distribution functions at each of the four edges with moment boundary conditions, nine moments have to be chosen. As an example, we will consider a south west edge, where the moment groups are given in from Table (2) in the appendix. We impose the following conditions;

$$\begin{aligned} &\rho u_x = 0, \rho u_y = \rho u_s, \rho u_z = 0, \\ &\Pi_{xx} = \frac{\rho}{3}, \quad \Pi_{yy} = \frac{\rho}{3} + \rho u_s^2, \quad \Pi_{zz} = \frac{\rho}{3}, \\ &\Pi_{xy} = -\tau \frac{\rho}{3} \partial_x u_y, \quad \Pi_{xz} = 0, \quad Q_{xyy} = \tau \frac{\rho}{3} \left((\partial_x u_y) \, u_y \right) \end{aligned}$$

In the above we have used the fact that the equilibrium and first order correction to the third moment Q_{xyy} are

$$Q^0_{xyy} = \frac{\rho}{3} u_x = 0, \quad Q^1_{xyy} = \frac{\rho}{3} \left((\partial_x u_y) \, u_y \right) \tag{31}$$

Upon converting to "barred" moments and solving for the unknown incoming $\overline{f}_i$we find that

$$\begin{aligned}
\overline{f}_1 &= \overline{f}_2 + 2\overline{f}_6 + 4\overline{f}_{13} + 2\overline{f}_{16} + 2\overline{f}_{17} - \frac{\rho}{3} - \frac{\rho\,(2\tau+1)}{6}\frac{u_s^2}{L_s},\\
\overline{f}_5 &= 2\overline{f}_2 + \overline{f}_3 + \overline{f}_4 + \overline{f}_6 + 4\overline{f}_8 + 4\overline{f}_9 + 4\overline{f}_{13} + 2\overline{f}_{16} + 2\overline{f}_{17} - \frac{2}{3}\rho\\
&\quad + \Delta t\rho g_y u_s - \rho u_s^2 + \frac{\rho\,(2\tau+1)}{6}\frac{u_s^2}{L_s},\\
\overline{f}_7 &= \overline{f}_8 + \frac{\rho\,(2\tau+1)}{12}\frac{u_s^2}{L_s} - \frac{\rho\,(2\tau+1)}{12}\frac{u_s}{L_s},\\
\overline{f}_{10} &= \overline{f}_9 + \frac{\rho\,(2\tau+1)}{12}\frac{u_s^2}{L_s} + \frac{\rho\,(2\tau+1)}{12}\frac{u_s}{L_s},\\
\overline{f}_{11} &= -\overline{f}_2 - \overline{f}_6 - \overline{f}_8 - \overline{f}_9 - 3\overline{f}_{13} - \overline{f}_{16} - \overline{f}_{17} + \frac{\rho}{3},\\
\overline{f}_{12} &= -\overline{f}_6 - \overline{f}_{13} - \overline{f}_{16} - \overline{f}_{17} + \frac{\rho}{6},\\
\overline{f}_{14} &= -\overline{f}_2 - \overline{f}_8 - \overline{f}_9 - \overline{f}_{13} + \frac{\rho}{6},
\end{aligned}$$

$$\begin{aligned}
\overline{f}_{15} &= -\overline{f}_3 - 2\overline{f}_8 - \overline{f}_{16} + \frac{\rho}{6} - \frac{\Delta t}{4}\rho g_y - \frac{\Delta t}{2}\rho g_y u_s + \frac{1}{2}\rho u_s + \frac{1}{2}\rho u_s^2,\\
&\quad - \frac{\rho\,(2\tau+1)}{12}\frac{u_s^2}{L_s} + \frac{\rho\,(2\tau+1)}{12}\frac{u_s}{L_s},\\
\overline{f}_{18} &= -\overline{f}_4 - 2\overline{f}_9 - \overline{f}_{17} + \frac{\rho}{6} + \frac{\Delta t}{4}\rho g_y - \frac{\Delta t}{2}\rho g_y u_s - \frac{1}{2}\rho u_s + \frac{1}{2}\rho u_s^2,\\
&\quad - \frac{\rho\,(2\tau+1)}{12}\frac{u_s^2}{L_s} - \frac{\rho\,(2\tau+1)}{12}\frac{u_s}{L_s}.
\end{aligned} \tag{32}$$

and the density is found from the known distribution functions by using this form $\rho - \rho\overline{u}_z$ which is depended on the definition of density $\rho = \overline{f}_0 + \overline{f}_1 + \overline{f}_2 + \overline{f}_3 + \overline{f}_4 + \overline{f}_5 + \overline{f}_6 + \overline{f}_7 + \overline{f}_8 + \overline{f}_9 + \overline{f}_{10} + \overline{f}_{11} + \overline{f}_{12} + \overline{f}_{13} + \overline{f}_{14} + \overline{f}_{15}\overline{f}_{16} + \overline{f}_{17} + \overline{f}_{18}$ and $\rho\overline{u}_z = \overline{f}_5 - \overline{f}_6 + \overline{f}_{11} - \overline{f}_{12} - \overline{f}_{13} + \overline{f}_{14} + \overline{f}_{15} - \overline{f}_{16} - \overline{f}_{17} + \overline{f}_{18}$. Thus, the density at the edge is

$$\rho = \overline{f}_0 + 2\overline{f}_2 + \overline{f}_3 + \overline{f}_4 + 2\overline{f}_6 + 2\overline{f}_8 + 2\overline{f}_9 + 4\overline{f}_{13} + 2\overline{f}_{16} + 2\overline{f}_{17}. \tag{33}$$

The slip velocity is once again found using the shear stress Π_{yz} and the relations $\Pi_{yz} = -\mu\partial_y u_{wall}$ and $u_s = -\dfrac{L_s}{\mu}\Pi_{yz}$. Thus at the south west edge we have

$$u_s = \frac{6L_s}{\rho(6L_s + 4\tau + 2)}\left(\frac{\Delta t}{2}\rho g_y + \overline{f}_3 - \overline{f}_4 + 2\overline{f}_8 - 2\overline{f}_9 + 2\overline{f}_{16} - 2\overline{f}_{17}\right). \tag{34}$$

4.2. The exact solution under Navier-slip boundary conditions

The analytical solution to this flow with Navier-slip boundary conditions at the four walls is [1]

$$u_y(x,z) = U_c\left[\sum_{n=1}^{\infty} D_n \cosh(A_3\beta_n z)\cos(\beta_n x) - \frac{4x^2 - 1 - 4A_1L_n}{A_1^2 8}\right], \tag{35}$$

where x is defined as $x = (i/n_x) - 0.5$, $i = 0, ..., n_x$, $z = (l/n_z) - 0.5$, $l = 0, ..., n_z$, $A_2 = \dfrac{D_h}{W}$, $A_1 = \dfrac{D_h}{H}$, $A_3 = \dfrac{A_1}{A_2}$, $Re = \dfrac{\rho_0 U_c D_h}{\mu}$ in which $D_h = \dfrac{2WH}{W+H}$ is the hydrodynamic diameter, the dimensionless slip length is $L_n = \dfrac{L_s}{D_h}$. The coefficients D_n are

$$D_n = \frac{4\sin(\frac{1}{2}\beta_n)}{A_1^2\beta_n^2\left[A_1\beta_n\theta_u L_n \sinh(\frac{1}{2}A_4\beta_n) + \cosh(\frac{1}{2}A_4\beta_n)\right]}\frac{1}{\sin(\beta_n)+\beta_n}, \tag{36}$$

where β_n are roots for $\beta_n \tan(\beta_n) = \dfrac{1}{A_1\beta_n L_n}$.

4.3. Numerical results

The relaxation times are given in lattice units where $\Delta_x = \Delta_t = 1$. The flow is driven by the body force $g_y = (U_c\nu {D_h}^2)$ in the y-direction. The simulated velocity profile is compared with the exact solutions. Navier-slip boundary conditions are implemented using moment-based boundary conditions at the North, South, West and East walls, and periodic boundary conditions used at the inlet and outlet *i.e.* Figure 7. These are used to simulate incompressible flow with wall slip with a slip length in the range $0.001 < L_n < 0.1$, as shown in Figure 8. Using a diffusive scaling we achieve second order accuracy second order accuracy for all studied relation times and slip lengths, as shown in Figure 9. Also, the centreline velocity is $U_c = 0.1$ and grid sizes in x and z-direction are $n_x = n_z = 16, 32, 64, 128$, and the grid sizes in y-direction is $n_y = 2$. The aspect ratio is unity, so the hydrodynamic diameter is $D_h = H$. The velocity profile is examined at the centreline of the channel *i.e.* at $n_x/2$ and $n_z/2$.

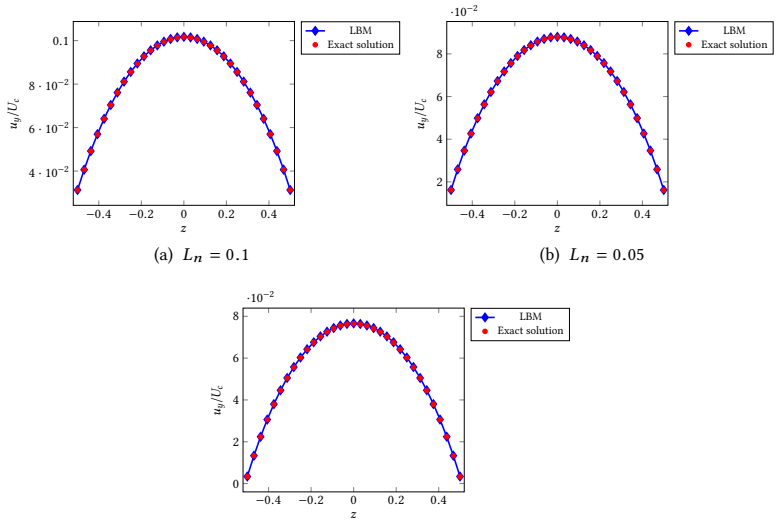

(a) $L_n = 0.1$ (b) $L_n = 0.05$

(c) $L_n = 0.01$

Figure 8. The velocity profile u_y at $\tau = 0.6$ and $n_x = n_z = 32$.

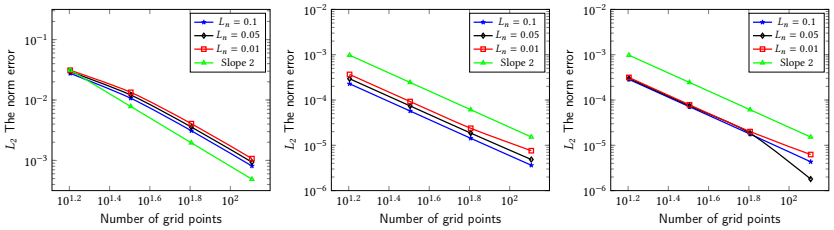

(a) $\tau = 6$ (b) $\tau = 0.6$ (c) $\tau = 0.1$

Figure 9. The norm error at different τ and L_n.

5. Conclusion

We have proposed for the first time moment-based boundary conditions for Navier slip condition in three dimensional lattice Boltzmann models. The method required the use of the third velocity moment to find the incoming distribution functions at edges and corners. Due to the truncation error in the non-conserved moments, there is an $O(\tau^2)$ error in the slip implementation. This is shown within our convergence studies, but this is within the order of accuracy of the LBM. Using a single relaxation time LBM, the results have been shown to be in excellent agreement with analytical solution and converge with second order accuracy. Future work will consider extending the method to micro scale flows, where the slip length is not an independent parameter but a function of the Knudsen number (viz., the relaxation time).

The Navier slip boundary condition is essential in the study of drag-reducing surfaces for accurately simulating flows over superhydrophobic surfaces or slippery liquid-infused surfaces (SLIPS). These advanced surface coatings create conditions where fluids effectively "slip" along the boundary, significantly reducing friction in ducts and pipes. By incorporating Navier slip boundary condition into Lattice Boltzmann

Method (LBM) simulations, researchers can quantify the extent of slip and evaluate its impact on energy efficiency. This capability supports the design of low-drag technologies for applications such as industrial piping, marine transport, and microchannel heat exchangers [10, 35].

In biomedical applications particularly in modeling blood flow through small capillaries or artificial vascular grafts the presence of surface coatings or biological structures such as the endothelial glycocalyx can give rise to apparent slip at the vessel wall. Incorporating Navier slip conditions into the lattice Boltzmann method allows for more realistic representation of these effects, leading to improved predictions of shear stress and cellular interactions in microcirculatory flow studies [40].

In addition, implementing slip boundary conditions within the lattice Boltzmann method has become increasingly important for simulating fluid-solid interactions at small scales or on surfaces with specialized properties. This paper is a step towards a viable method. A key related application area is microfluidic devices such as lab-on-a-chip systems where fluid flows are confined to micrometer-scale channels. At these scales, the traditional no-slip boundary condition often fails to capture observed behaviours, especially near hydrophobic or superhydrophobic walls. Experimental studies have shown that nanoengineered surfaces can induce measurable slip, resulting in reduced drag and enhanced flow rates [10]. Incorporating slip conditions into LBM enables more accurate modeling of these effects, allowing for better predictions of flow rates, pressure drops, and fluid mixing factors that are critical for applications in biomedical diagnostics and chemical assays [40].

We discussed in the text that the moment-based method has the current shortcoming of being applicable only to regular geometries. Overcoming this hurdle is important future work, but not within the scope of this paper. Avenues worth exploring to improve geometric flexibility include interpolation-based approached to apply conditions on boundaries that are projected to the nearest grid point. The interpolation length may be analogous to a slip length. While this would be a major development, the ability to apply boundary conditions accurately and locally and grid points aligned with lattice nodes in still a success of the moment-based approach. With specific reference to the slip flow considered here, we can impose Neumann conditions without any additional finite difference approximations, without any tuning of free parameters, without needed to adjust the collision operator to eliminate slip errors, and without calibrating the method against other solutions to optimise accuracy.

Moment-based boundary conditions offer the potential to accurately impose complicated boundary conditions at grid points, while providing enhanced stability at high Reynolds numbers with more sophisticated collision operators [24], making them well-suited for applications in microfluidics and biomedical flows. By extending the methodology to three dimensional flows in the presence of slip, we offer the prospect of using the LBM with moment-based boundary conditions to study a greater volume of flow problems. The reach of the method will increase further when it is developed for efficient simulations in complex geometries.

References

[1] K. Al Khasawneh, H. Liu, and C. Cai, *Asymptotic Solutions for Gaseous Flow in a Three-Dimensional Rectangular Microchannel*, in *49th AIAA Aerospace Sciences Meeting including the New Horizons Forum and Aerospace Exposition*. 2011, p. 181.

[2] R. Allen and T. Reis, *Moment-based boundary conditions for lattice Boltzmann simula-*

tions of natural convection in cavities, Prog. Com. Fluid Dyn, an International Journal 16 (2016), pp. 216–231.

[3] S. Ansumali and I.V. Karlin, *Kinetic boundary conditions in the lattice Boltzmann method*, Phys. Rev. E 66 (2002), p. 026311.

[4] R. Bazarin, P. Philippi, A. Randles, and L. Hegele Jr, *Moments-based method for boundary conditions in the lattice boltzmann framework: A comparative analysis for the lid driven cavity flow*, Computers & Fluids 230 (2021), p. 105142.

[5] S. Bennett, *A lattice Boltzmann model for diffusion of binary gas mixtures*, Ph.D. diss., University of Cambridge, 2010.

[6] A. Bertozzi, M. Shearer, and R. Buckingham, *Thin film traveling waves and the Navier slip condition*, SIAM J. Appl. Math. 63 (2003), pp. 722–744.

[7] Z. bu Sinnah, *Lattice Boltzmann method for 2D and 3D flows in channels and ducts with slip and no-slip wall*, Ph.D. diss., Plymouth University, 2020.

[8] Z. Chai, Z. Guo, L. Zheng, and B. Shi, *Lattice Boltzmann simulation of surface roughness effect on gaseous flow in a microchannel*, Journal of Applied Physics 104 (2008), p. 014902. Available at https://doi.org/10.1063/1.2949273.

[9] Z. Chai, B. Shi, Z. Guo, and F. Rong, *Multiple-relaxation-time lattice Boltzmann model for generalized newtonian fluid flows*, Journal of Non-Newtonian Fluid Mechanics 166 (2011), pp. 332–342. Available at https://doi.org/10.1016/j.jnnfm.2011.01.002.

[10] C. Choi and C.J. Kim, *Large slip of aqueous liquid flow over a nanoengineered superhydrophobic surface*, Physical Review Letters 96 (2006), p. 066001.

[11] D. d'Humières and I. Ginzburg, *Viscosity independent numerical errors for lattice Boltzmann models: From recurrence equations to "magic" collision numbers*, Comput. Math. Applic. 58 (2009), pp. 823–840.

[12] M. Fang, R. Gilbert, and X. Liu, *A squeeze flow problem with a Navier slip condition*, Math. Comput. Modelling 52 (2010), pp. 268–277.

[13] I. Ginzbourg and P. Adler, *Boundary flow condition analysis for the three-dimensional lattice Boltzmann model*, J. Phys. II 4 (1994), pp. 191–214.

[14] I. Ginzburg, F. Verhaeghe, and D. d'Humières, *Study of simple hydrodynamic solutions with the two-relaxation-times lattice Boltzmann scheme*, Commun. Comput. Phys. 3 (2008), pp. 519–581.

[15] I. Ginzburg, F. Verhaeghe, and D. d'Humières, *Two-relaxation-time lattice Boltzmann scheme: About parametrization, velocity, pressure and mixed boundary conditions*, Commun. Comput. Phys. 3 (2008), pp. 427–478.

[16] W. Guo and G. Hou, *Novel schemes of no-slip boundary conditions for the discrete unified gas kinetic scheme based on the moment constraints*, Entropy 25 (2023), p. 780.

[17] X. He, X. Shan, and G.D. Doolen, *Discrete Boltzmann equation model for nonideal gases*, Phys. Rev. E 57 (1998), p. R13.

[18] X. He, Q. Zou, L.S. Luo, and M. Dembo, *Analytic solutions of simple flows and analysis of nonslip boundary conditions for the lattice Boltzmann BGK model*, J. Stat. Phys 87 (1997), pp. 115–136.

[19] S. Jiménez Bolaños and B. Vernescu, *Derivation of the Navier slip and slip length for viscous flows over a rough boundary*, Phys Fluids 29 (2017), p. 057103.

[20] A. Khaled and K. Vafai, *The effect of the slip condition on stokes and couette flows due to an oscillating wall: Exact solutions*, International Journal of Non-Linear Mechanics 39 (2004), pp. 795–809.

[21] I. Krastins, A. Kao, K. Pericleous, and T. Reis, *Moment-based boundary conditions for straight on-grid boundaries in three dimensional lattice Boltzmann simulations*, Int. j. for Numerical Methods in Fluids 92 (2020), pp. 1948–1974.

[22] C.Y. Lim, C. Shu, X.D. Niu, and Y.T. Chew, *Application of lattice Boltzmann method to simulate microchannel flows*, Phys. fluids 14 (2002), pp. 2299–2308.

[23] L.S. Luo, *Unified theory of lattice Boltzmann models for nonideal gases*, Phys. Rev. Lett. 81 (1998), p. 1618.

[24] S. Mohammed, D. Graham, and T. Reis, *Assessing moment-based boundary conditions*

for the lattice Boltzmann equation: A study of dipole-wall collisions, Comput & Fluids 176 (2018), pp. 79–96.

[25] S. Mohammed, D. Graham, and T. Reis, *Modeling the effects of slip on dipole–wall collision problems using a lattice Boltzmann equation method*, Phys. Fluids 32 (2020), p. 025104.

[26] S. Mohammed and T. Reis, *A lattice Boltzmann method with moment-based boundary conditions for rarefied flow in the slip regime,*, Phys. Rev. E 104 (2021), p. 045309.

[27] C.L.M.H. Navier, *Mémoire sur les lois du mouvement des fluides*, Mémoires de l'Académie R. des Sci. de l'Institut de France 6 (1823), pp. 389–440.

[28] D.R. Noble, S. Chen, J.G. Georgiadis, and R.O. Buckius, *A consistent hydrodynamic boundary condition for the lattice Boltzmann method*, Phys. Fluids 7 (1995), pp. 203–209.

[29] A.V. Pillai and K.V. Manu, *Analytical solutions for unsteady pipe flows with slip boundary condition*, Journal of Applied Fluid Mechanics 13 (2020), pp. 1015–1026.

[30] T. Reis, *Burnett order stress and spatially-dependent boundary conditions for the lattice Boltzmann method*, Commun. Comput. Phys 27 (2020), pp. 167–197.

[31] T. Reis and P.J. Dellar, *Moment-based formulation of Navier–Maxwell slip boundary conditions for lattice Boltzmann simulations of rarefied flows in microchannels*, Phys. Fluids (2012).

[32] T. Reis, *On the lattice Boltzmann deviatoric stress: analysis, boundary conditions, and optimal relaxation times*, SIAM J. Sci. Comput. 42 (2020), pp. B397–B424.

[33] R. Samanta, M. Sultan, and H. Chattopadhyay, *Flow-field in a lid driven cavity with slip boundaries: An investigation using lattice boltzmann modelling*, Chemical Engineering Science 273 (2023), p. 118661. Available at https://doi.org/10.1016/j.ces.2023.118661.

[34] O. San and A.E. Staples, *Dynamics of pulsatile flows through elastic microtubes*, International Journal of Applied Mechanics 4 (2012), pp. 1369–1383. Analytical solution including Navier-slip boundary conditions.

[35] M. Sbragaglia, R. Benzi, L. Biferale, S. Succi, and F. Toschi, *Generalized navier boundary condition and slip flow in hydrophobic microchannels*, Physical Review Letters 97 (2006), p. 204503.

[36] G. Silva, *Consistent lattice Boltzmann modeling of low-speed isothermal flows at finite Knudsen numbers in slip-flow regime.ii. application to curved boundaries*, Phys. Rev. E. 98 (2018), p. 023302.

[37] G. Silva and I. Ginzburg, *Slip velocity boundary conditions for the lattice Boltzmann modeling of microchannel flow*, Int. J. Num. Methods Fluids 94 (2022), pp. 2104–2136.

[38] G. Silva and V. Semiao, *Consistent lattice Boltzmann modeling of low-speed isothermal flows at finite Knudsen numbers in slip-flow regime: Application to plane boundaries*, Phys. Rev. E. 96 (2017), p. 013311.

[39] Z.A.B. Sinnah, D.I. Graham, and T. Reis, *Lattice Boltzmann modelling of pulsatile flow using moment boundary conditions*, in *Proceedings of the 6th European Conference on Computational Mechanics and 7th European Conference on Computational Fluids Dynamics*. 2012.

[40] S. Succi, *The lattice Boltzmann equation: for fluid dynamics and beyond*, Oxford University Press,Oxford, 2001.

[41] S. Succi, *Mesoscopic modeling of slip motion at fluid-solid interfaces with heterogeneous catalysis*, Phys Rev. Lett 89 (2002), p. 064502.

[42] G.H. Tang, W.Q. Tao, and Y.L. He, *Lattice Boltzmann method for gaseous microflows using kinetic theory boundary conditions*, Phys. Fluids 17 (2005), p. 058101.

[43] S. Tao, X. Zhang, W. Wang, L. Wang, Q. He, and Y. Lin, *Bifurcate migration of neutrally buoyant particles in unilateral slippery channel flows*, Physics of Fluids 36 (2024), p. 103307. Available at https://doi.org/10.1063/5.0230847.

[44] F. Verhaeghe, L. Luo, and B. Blanpain, *Lattice Boltzmann modeling of microchannel flow in slip flow regime*, J. of Comput Phys 228 (2009), pp. 147–157.

[45] J.R. Womersley, *Method for the calculation of velocity, rate of flow and viscous drag in arteries when the pressure gradient is known*, The Journal of physiology 127 (1955), p.

553.

6. Appendix

Table 1. Moments at the South boundary, in 3D.

Moments	Combination of unknown distribution functions at the South boundary
$\rho u_x, \Pi_{xz}, Q_{xzz}$	$f_{11} - f_{14}$
$\rho u_y, \Pi_{yz}, Q_{yzz}$	$f_{15} - f_{18}$
$\rho, \rho u_z, \Pi_{zz}$	$f_5 + f_{11} + f_{14} + f_{15} + f_{18}$
$\Pi_{xx}, R_{xxzz}, Q_{xxz}$	$f_{11} + f_{14}$
$\Pi_{yy}, R_{yyzz}, Q_{yyz}$	$f_{15} + f_{18}$

Table 2. Moments at the South West edge, in 3D.

Moments	Combination of unknown distribution functions at the South West edge
ρ	$f_1 + f_5 + f_7 + f_{10} + f_{11} + f_{12} + f_{15} + f_{16}$
$\rho u_x, \Pi_{xx}$	$f_1 + f_7 + f_{10} + f_{11} + f_{12}$
ρu_y	$f_7 - f_{10} + f_{15} - f_{18}$
ρu_z	$f_5 + f_{11} - f_{12} + f_{15} + f_{18}$
Π_{yy}	$f_7 + f_{10} + f_{15} + f_{18}$
Π_{zz}	$f_5 + f_{11} + f_{12} + f_{15} + f_{18}$
Π_{xy}, Q_{xxy}	$f_7 - f_{10}$
Π_{xz}, Q_{xxz}	$f_{11} - f_{12}$
Q_{xyy}	$f_7 + f_{10}$
Π_{yz}, Q_{yzz}	$f_{15} - f_{18}$
Q_{xzz}	$f_{11} + f_{12}$
Q_{yyz}, R_{yyzz}	$f_{15} + f_{18}$
R_{xxyy}	$f_{10} + f_{11}$
R_{xxzz}	$f_{12} + f_{15}$

Table 3. Moments at the South West front corner, in 3D.

Moments	Combination of unknown distribution functions at South West front corner
ρ	$f_1 + f_3 + f_5 + f_7 + f_8 + f_{10} + f_{11} + f_{12} + f_{14} + f_{15} + f_{16} + f_{18}$
ρu_x	$f_1 + f_7 - f_8 - f_9 + f_{10} + f_{11} + f_{12} - f_{14}$
ρu_y	$f_3 + f_7 + f_8 - f_{10} + f_{15} + f_{16} - f_{18}$
ρu_z	$f_5 + f_{11} - f_{12} + f_{14} + f_{15} - f_{16} + f_{18}$
Π_{xx}	$f_1 + f_7 + f_8 + f_9 + f_{10} + f_{11} + f_{12} + f_{14}$
Π_{yy}	$f_3 + f_7 + f_8 + f_{10} + f_{15} + f_{16} + f_{18}$
Π_{zz}	$f_5 + f_{11} + f_{12} + f_{14} + f_{15} + f_{16} + f_{18}$
Π_{xy}	$f_7 - f_8 - f_{10}$
Π_{xz}, Q_{xzz}	$f_{11} - f_{12} - f_{14}$
Π_{yz}	$f_{15} - f_{16} - f_{18}$
Q_{xxy}	$f_7 + f_8 - f_{10}$
Q_{xyy}	$f_7 - f_8 + f_{10}$
Q_{yzz}	$f_{15} + f_{16} - f_{18}$
Q_{xxz}	$f_{11} - f_{12} + f_{14}$
Q_{yyz}	$f_{15} - f_{16} + f_{18}$
R_{xxyy}	$f_8 + f_{10} + f_{11}$
R_{xxzz}	$f_{12} + f_{14} + f_{15}$
R_{yyzz}	$f_{15} + f_{16} + f_{18}$

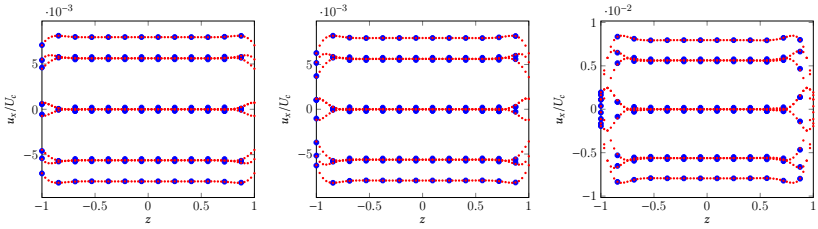

(a) $L_n = 0.388$ (b) $L_n = 0.194$ (c) $L_n = 0.0194, 0$

Figure 1. Pulsatile flow with slip on coarser grids. Blue: velocity profile of LBM; Red: velocity profile of exact solution at $\tau = 0.6$ and $n_x = n_y = 2$, $n_z = 64$. (a), (b) and (c) for $W_0 = 11.201$.

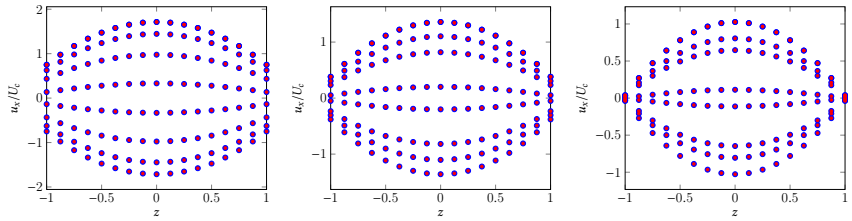

(a) $L_n = 0.388$ (b) $L_n = 0.194$ (c) $L_n = 0.0194, 0$

Figure 2. Pulsatile flow with slip on coarser grids. Blue: velocity profile of LBM; Red: velocity profile of exact solution at $\tau = 0.6$ and $n_x = n_y = 2$, $n_z = 16$. (a), (b) and (c) for $W_0 = 0.3544$.